DIAGNOSTYKA, 2017, Vol. 18, No. 1

ISSN 1641-6414
e-ISSN 2449-5220

EXPERIMENTAL INVESTIGATION OF CERAMIC BALL BEARINGS FOR MICROTURBINES

Paweł BAGIŃSKI, Artur ANDREARCZYK, Grzegorz ŻYWICA
Institute of Fluid Flow Machinery, Polish Academy of Sciences
pbaginski@imp.gda.pl, aandrearczyk@imp.gda.pl, gzywica@imp.gda.pl

Abstract

This article presents the experimental research on ball bearings, which could be applied in vapour microturbines operating in CHP systems. The bearings are of three kinds, according to their constructional solution: 1. all-steel (all components are made of steel); 2. ceramic-steel-hybrid (ceramic balls, steel cage and races); 3. all-ceramic (the balls, as well as external and internal races, are made from ceramic silicon nitride – Si_3N_4, while the cage is made of PTFE). The test rig and the research method were discussed. In order to have a better picture of vibrations of the rotor-bearing system, we applied the bearing system with a flexible rotor. That option entailed some difficulties, however. In each case, both the analysis of the ball bearings' properties and of the impact of ceramic components on the dynamic performance of the rotor was carried out. The results of these analyses are presented in the following forms: displacement amplitudes of the rotor, colormap graphs of the type Order Spectrum Analysis and three-dimensional vibration trajectories. The bearings were analysed on the basis of colormap graphs, while the analysis of the rotating rotor was conducted using graphs depicting 3D vibration trajectories and displacement amplitudes at the disk location. As a result of all this work that we have mentioned, useful information on the possible application of tested bearings for vapour microturbines has been gained.

Keywords: ball bearings, ceramic bearings, hybrid bearings, rotor dynamics

BADANIA EKSPERYMENTALNE CERAMICZNYCH ŁOŻYSK TOCZNYCH STOSOWANYCH W MIKROTURBINACH

Streszczenie

W artykule przedstawiono opis badań trzech rodzajów łożysk kulkowych, które mogłyby być zastosowane w mikroturbinach parowych pracujących w układach kogeneracyjnych. Rodzaje badanych łożysk to: stalowe, hybrydowe (kulki ceramiczne, bieżnie stalowe, koszyk stalowy, ceramiczne gdzie elementy takie jak bieżnie wew. i zew. oraz kulki zostały wykonane z azotku krzemu (Si_3N_4) a koszyk z PTFE. Opisano budowę stanowiska badawczego i metodę badań. Aby drgania układu wirnik – łożyska były lepiej widoczne zastosowano wiotki wirnik, co sprawiało dodatkowe trudności podczas badań. W każdym z przypadków porównano właściwości badanych łożysk tocznych oraz wpływ elementów ceramicznych na dynamikę wirnika. Wyniki te przedstawiono w formie przebiegów, histogramów (Order Spectrum Analysis) i wykresów trajektorii drgań. Na podstawie map ekspozycji przeprowadzono analizę łożysk natomiast za pomocą przebiegów amplitudy przemieszczenia dysku i trajektorii 3D analizę wirującego wiotkiego wirnika. W rezultacie oceniono możliwość zastosowania badanych łożysk w mikroturbinach parowych.

Słowa kluczowe: łożyska kulkowe, łożyska ceramiczne, łożyska hybrydowe, dynamika wirnika

1. INTRODUCTION

One of the subassemblies comprising a micro CHP power plant, which is being developed at the Institute of Fluid-Flow Machinery PAN [1, 2], is the vapour microturbine [3, 4]. Due to harsh operating conditions (including high rotational speed, difficulties in using traditional lubricants and high temperature), there is a need to apply unconventional bearings to the microturbine (e.g. gas or foil bearings) [5–7]. Ball bearings—all-steel, all-ceramic or ceramic-steel-hybrid ones—can be a simpler, cost-effective alternative.

One important area where knowledge is lacking is the possibility of using a rotor supported by ceramic or hybrid bearings. As a matter of fact, there are virtually no articles in the scientific literature addressing this subject. Usually, a research aimed at studying issues of ceramic-metal-hybrid bearings or all-ceramic bearings is related to analysing a single bearing only. In publications relating to such bearings, researchers were faced with the issues of extreme temperatures (very low or very high), life cycle, wear, mechanical friction, material selection, vibration resistance, etc. For example, article [8] discusses the research conducted on two bearing designs, where one of them has ceramic balls in the place of steel balls. When tested in the single ball test rig at a high rotational speed, the ceramic balls exhibited a

quadruple rolling contact fatigue life improvement versus steel balls. This research gave new impetus to the improvement of bearing systems mounted in high-speed machinery. Many analyses related to the wearing of the rolling elements of ceramic bearings were carried out [8–10] and they show that such bearings are suitable for machines operating under demanding conditions. Article [11] presents a vibration analysis of a single ceramic bearing and its comparison with steel bearings. During the experiment, a bearing was operated at several different speeds (and loads as well) and for each case, vibration characteristics were registered. Vibrations were measured using accelerometers. It was established that the hybrid bearings had higher vibration level than steel bearings. It was due to the fact that there was a higher contact stiffness between the ceramic rolling elements and the races in comparison to steel rolling elements and steel races. In the research concerning the use of hybrid ceramic bearings for rocket turbopumps having a nominal speed of 50,000 rpm [12-13] and automobile turbochargers [14], a single bearing test rigs had been constructed on which various bearing types were tested. The parameters such as load capacity and life cycle were analysed, for ceramic-metal-hybrid bearings and all-ceramic bearings as well. Paper [15] discusses the research on a rotor supported by two ceramic bearings. This paper provides no information either on vibration level of the rotor or on its displacements. The authors concentrate on such issues as heat generation and temperature rises as well as oil shut-off tests. Some of the advantages of hybrid bearings were demonstrated but the impact of vibrations on the dynamic performance of the rotor–bearings system was not taken into account. The simulational vibration analysis of ceramic ball bearings applied to a 10 kW turbine is the subject of article [16].

The authors of this article conducted experimental research on a rotor supported by various types of ball bearings. The possibility of using such bearings in a prototypical vapour microturbine was discussed. Properties of ceramic-metal-hybrid and all-ceramic bearings, described in the scientific journals, allow us to put forward the thesis that ceramic ball bearings can be a great alternative to other types of bearings that are usually used in energy microturbines' bearing systems. The all-steel ball bearings were taken into account because they make reference to the other two bearing kinds that were tested and also because they are frequently applied to high-speed systems.

2. TEST RIG AND RESEARCH METHOD

2.1. General description of the test rig

Figure 1 shows the scheme on which are marked the overall dimensions of the test rig. For the purposes of the research presented in this article, two elements were manufactured, namely the shaft and the rotor disk, the total mass of which is 3.5 kg. The distance between the bearing supports is 727 mm, while the shaft diameter is 20 mm along its whole length. This configuration of the test rig—how later it will turn out—led to high displacements of the rotor disk. The rotor can be henceforth considered flexible.

An electric motor—incorporating a belt transmission—was connected to the shaft using a flexible jaw coupling. On the bearing supports, uniaxial accelerometers were mounted and they were capable of conducting measurements in two directions—X and Y. The rotational speed of the rotor was measured using a laser sensor and shaft displacements were measured at the rotor disk's location—in two mutually perpendicular directions—using eddy current sensors.

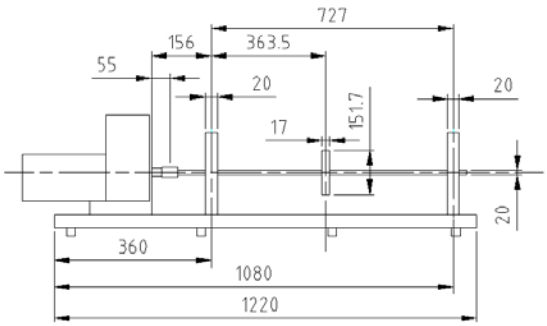

Fig. 1. Scheme of the test rig

The whole test apparatus was connected to the SCADAS Mobile analyser, the role of which was to register, process and validate signals from all sensors. All measurement parameters were set by means of Test.Lab Signature Testing software.

2.2. Course of the study

In the first test, the system included ball bearings in which all components were made of steel. All bearings operated without lubrication. Before starting the research and also after the substitution of each bearing the rotor was balanced using a portable vibration analyser called DIAMOND 401 (Fig. 2). Balancing was done by attaching an appropriate corrective mass to the shaft, according to the display of the vibration analyser so as to decrease the overall vibration level. The root-mean-square (RMS) vibration velocity value of 1 mm/s was the threshold value below which the rotor was considered balanced.

During the planning of a series of measurements, a proper positioning of eddy current sensors turned out to be a problem. The sensors have the measuring range of 0.5 mm to 2.5 mm and the vibration level of the flexible rotor was too high to be within this range. However, the problem has been overcome. The sensors were positioned in such a way that their arrangement did not allow damaging them, even at the resonant speed. During conducting the measurement series the following parameters were registered: rotational speed,

accelerations of the bearing supports in two directions perpendicular to the axis of rotation of the rotor and displacement of the shaft at the point that is close to the rotor disk's position.

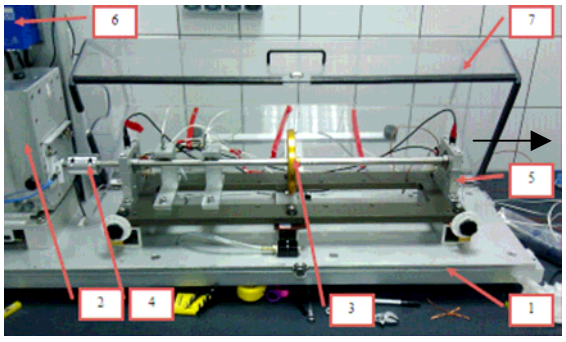

Fig. 2. Test rig for testing small rotor-bearings systems (in configuration with ball bearings). 1 – foundation, 2 – electric motor with the belt transmission, 3 – shaft with the rotor disk, 4 – permanent coupling, 5 – bearing support, 6 – frequency converter, 7 – protective guard

Each bearing replacement required the removal of the shaft and the coupling. After the replacement, the shaft had to undergo the balancing process from the beginning.

3. RESEARCH RESULTS

3.1. All-steel ball bearings (FAG 6204-C-2Z-C3)

This chapter discusses the measurement results registered during the run-up of the rotor supported by all-steel bearings. The graphs presented in Fig. 3-6 demonstrate acceleration amplitudes as the function of rotational speed shown in the form of its individual harmonics. The colormap graphs of the type Order Spectrum Analysis are hereinafter referred to as "OSA graphs". The amplitude values measured by accelerometers are colour coded. Thin curved lines are the frequencies expressed in hertz (Hz).

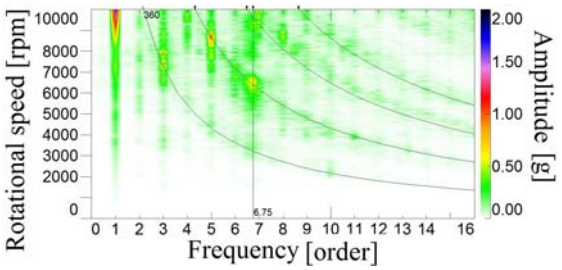

Fig. 3. OSA graph showing vibration acceleration amplitudes measured in the X direction at the first all-steel ball bearing support

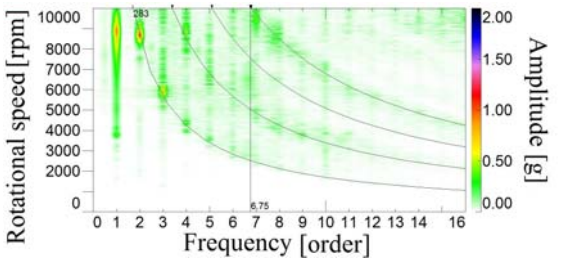

Fig. 4. OSA graph showing vibration acceleration amplitudes measured in the Y direction at the first all-steel ball bearing support

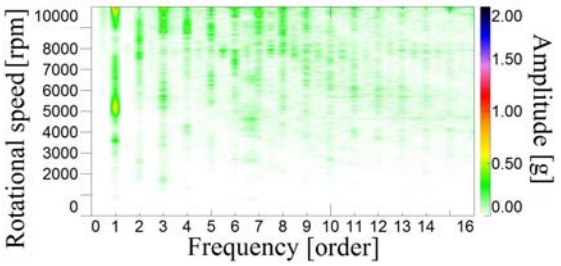

Fig. 5. OSA graph showing vibration acceleration amplitudes measured in the X direction at the second all-steel ball bearing support

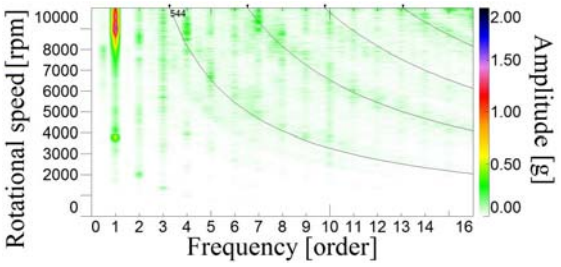

Fig. 6. OSA graph showing vibration acceleration amplitudes measured in the Y direction at the second all-steel ball bearing support

Figures 3-6 present the values measured at two bearing supports and in two directions. It can be noticed that for the first support (Fig. 3 and Fig. 4) the first harmonic component was dominant and the highest amplitude value (1.4 g) occurred at the maximal rotational speed. When the rotor passed the speed of 7,000 rpm, the third and fifth harmonics began to manifest themselves—which may be an indication of the bent shaft or, in the case of a flexible rotor, its unstable operation. It can be also observed that there is a high amplitude value at the frequency order of 6.75 (see Fig. 3) and this value originates from vibrations of the drive's belt transmission. Curved thin lines denote the resulting vibration amplitudes at the frequency of 360 Hz and its harmonics as well. These harmonics made a powerful contribution to causing unstable and unreliable operation of the mechanical system. This unstable operation manifested itself in the form of high vibration level at the bearing supports' locations [17]. At the first bearing support's location in the Y direction (Fig. 5), the first three harmonics (0.7 g, 0.85 g and 0.68 g, respectively) are present—which was a clear indication of the

operation of a bent rotor. The subsequent figures (Fig. 5 and Fig. 6) demonstrate the vibrations of the second bearing support. The vibration acceleration amplitude measured in the X direction was the highest (0.65 g) for the harmonic that is synchronous with the rotational speed of the rotor (Fig. 5). At higher speeds, the vibration acceleration amplitudes of the other harmonics increased. The vibrations of the test rig's structure, observed at the frequency of 283 Hz, contributed to the increase in vibration acceleration amplitudes registered at the bearings' locations. In the Y direction, the first harmonic is the dominant vibration component and its amplitude value (1.2 g) increases along with increasing the rotational speed, which can be observed in Fig. 6. Although vibrations of the test rig's structure could have been noticed at 544 Hz, they had virtually no impact on the operation of the rotor itself.

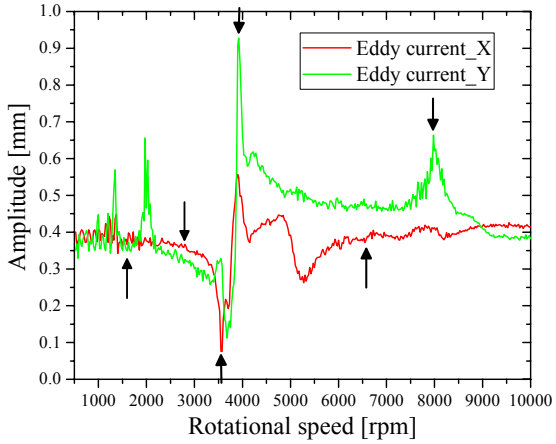

Fig. 7. Amplitude of the rotor's displacement measured at the disk's location (in the X and Y direction) vs. rotational speed

Figure 7 presents the amplitude of the rotor's displacement—measured by eddy current sensors—as the function of rotational speed. It can be noticed that at low rotational speeds the rotor moved towards the Y direction in a rapid, repetitive manner. A stable operation can be observed after passing through the speed of 2,100 rpm and it continues up to a resonant speed (3,924 rpm), where the highest displacements occurred (0.92 mm and 0.55 mm in the Y and X directions, respectively). After crossing the resonant speed, the amplitudes decreased but their values were higher than the amplitude value registered at the speed of 2,100 rpm.

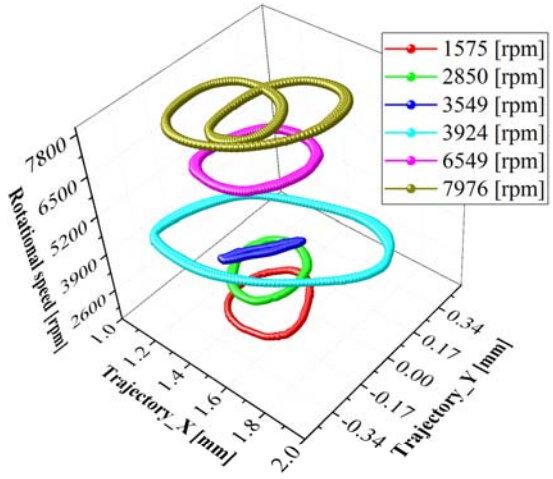

Fig. 8. Trajectories of absolute vibrations at different rotational speeds

The next figure (Fig. 8) depicts vibration trajectories of the rotor at various rotational speeds. The trajectories are presented using a 3D graph on which the horizontal plane represents the position of the shaft at a given speed. Z axis holds the values of rotational speeds. Common colour coding has been applied to certain rotational speeds, as shown in the legend. Such type of graph makes it possible to compare the shape of individual trajectories, while their size is better visible in Fig. 7. The amplitudes of the rotor's displacements measured at the disk were higher than those measured at the bearing supports, and this was the case for all rotational speeds. The six chosen rotational speeds that are colour coded in Fig. 8 are marked by arrows in Fig. 7. In Fig. 7, many amplitude peak values are present on the green curve. The vibration trajectories at all these speeds, apart from a resonant speed, are smaller in size but similar in shape to the trajectory registered at the speed of 7,976 rpm (see yellow trajectory in Fig. 8). The results described in this chapter should be considered as reference values to the values presented in the following chapters.

3.2. Ceramic-steel-hybrid ball bearings (S6204 2-RS)

The results relating to the ceramic-steel-hybrid ball bearings are presented in the same manner as the ones which have been described in the previous chapter. On the OSA graph shown in Fig. 9, the first harmonic is dominant (1.2 g) but also the third and fifth harmonics, as well as the component originating from vibrations of the drive, are visible. The vibrations of the bearing supports (360 Hz) had a negative impact on the operation of the rotor itself. The vibration acceleration amplitude registered at the second bearing support in the X direction (Fig. 11) is at a low level, as in the previous case.

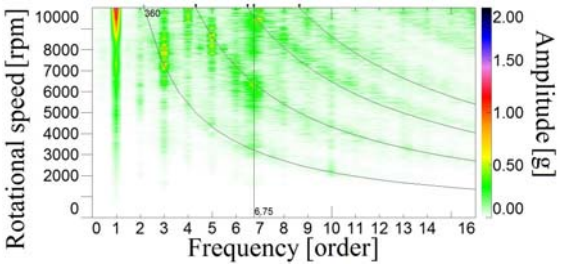

Fig. 9. OSA graph showing vibration acceleration amplitudes measured in the X direction at the first hybrid bearing support

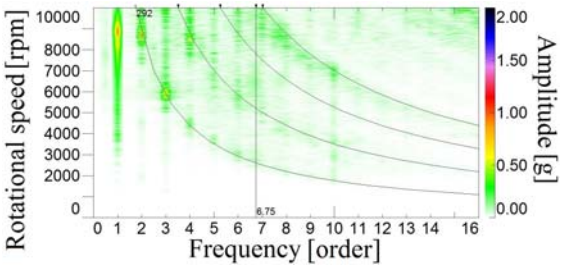

Fig. 10. OSA graph showing vibration acceleration amplitudes measured in the Y direction at the first hybrid bearing support

The vibrations measured in the Y direction (Fig.10) at the first bearing support are of similar nature to those from the previous case. The vibration acceleration amplitude of the first three spectrum components was approximately 0.7 g. The frequency value originating from vibrations of the test rig's structure increased to 292 Hz. At the second bearing support (Fig. 12), the vibration acceleration amplitude was 1.2 g, which is similar to the case with all-steel bearings.

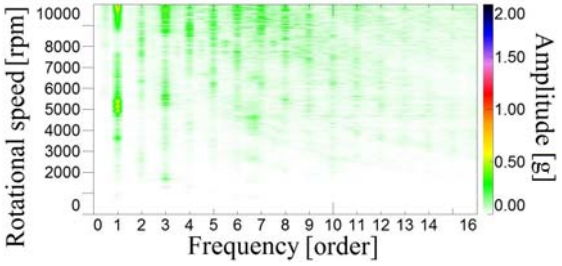

Fig. 11. OSA graph showing vibration acceleration amplitudes measured in the X direction at the second hybrid bearing support

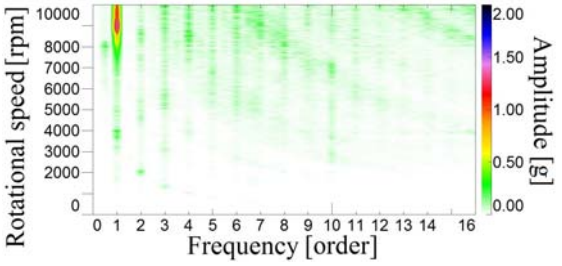

Fig. 12. OSA graph showing vibration acceleration amplitudes measured in the Y direction at the second hybrid bearing support

The bearings' vibrations are of a similar nature to those from the previous chapter. The highest registered amplitude of the rotor's displacement during the run-up was 1.22 mm and increased by 0.3 mm as compared to the reference value given in the previous chapter (Fig. 13). A stable operation starts above the speed of 2,100 rpm. After passing through a resonant speed, the amplitude value recovered to normal levels and oscillated around 0.5 mm). In the case of all-steel bearings, the vibration trajectories which had loops in their shapes were obtained for the rotational speeds at which the highest amplitudes of the rotor's displacements were registered and this was in the Y direction. However, in the case of ceramic-steel-hybrid bearings, we can say the same with one major difference – we have to exchange Y with X.

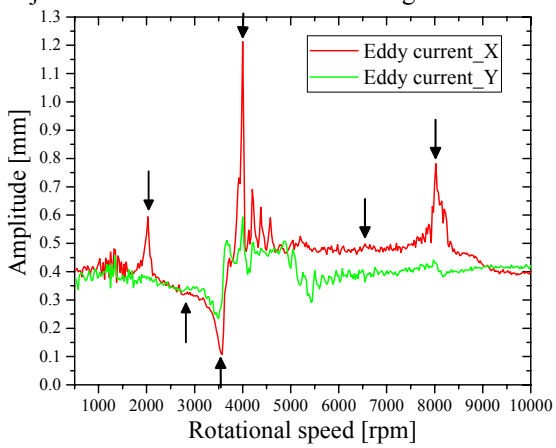

Fig. 13. Amplitude of the rotor's displacement measured at the disk's location (in the X and Y direction) vs. rotational speed

Vibration trajectories of the rotor are shown in Fig. 14. In this figure, the red thick line depicts the trajectory of the rotor operating at the rotational speed of 2,024 rpm, registered at the beginning of the run-up—during unstable operation (see the previous Fig. 13).

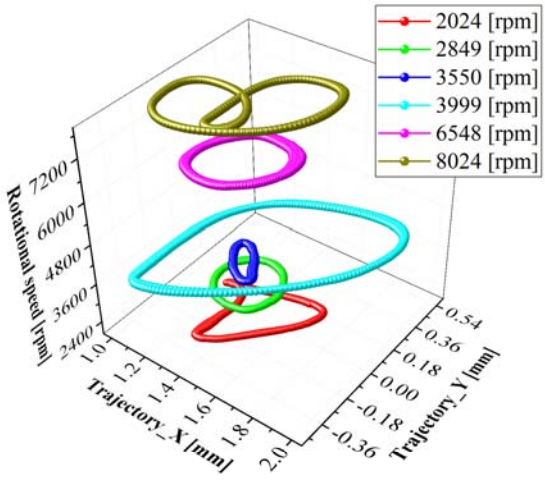

Fig. 14. Trajectories of absolute vibrations at different rotational speeds

A loop, visible in the shape of this trajectory, might have appeared due to too rapid increase in the rotational speed of the rotor.

The overall conclusion is that both the vibration trajectories are similar in shape and size as well as the amplitudes of the rotor's displacements are similar in values to those obtained for all-steel bearings. As we already mentioned during the analysis of the measurement results relating to ceramic-steel-hybrid bearings, a significant increase in vibration level at the resonant speed was observed which could be the result of worse damping properties of these bearings.

3.3. All-ceramic ball bearings (N620 T-LL)

The following graphs present vibrations of bearing supports in the case where the rotor was supported by all-ceramic bearings. In Fig. 15 we have presented the vibration acceleration amplitudes measured in the X direction at the first bearing support. The following vibration components are present in this figure: the first harmonic (1.3 g), the third harmonic (0.7 g), the fifth harmonic (1.1 g) and the component originating from vibrations of the drive. This time vibrations of the bearing supports were also observed (360 Hz) and have adversely affected the operation of the rotor itself. It is evident, particularly when looking at the values measured in the Y direction (Fig. 16), that vibrations of the test rig's structure (288 Hz and 576 Hz) caused the appearance of the vibration acceleration amplitudes corresponding to the second(0.62 g) third(0.72 g), fourth(0.5 g) and fifth (0.25 g) harmonics of the rotational speed of the rotor. The first harmonic (0.78 g) dominates over the whole range of rotational speeds.

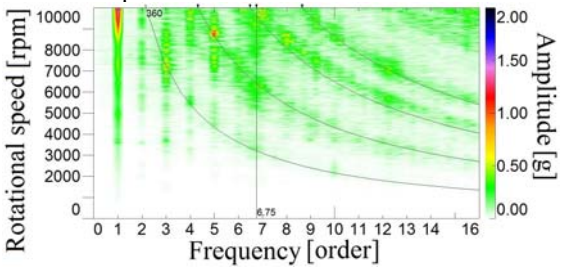

Fig. 15. OSA graph showing vibration acceleration amplitudes measured in the X direction at the first ceramic bearing support

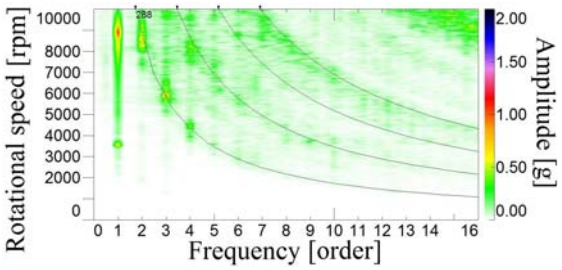

Fig. 16. OSA graph showing vibration acceleration amplitudes measured in the Y direction at the first ceramic bearing support

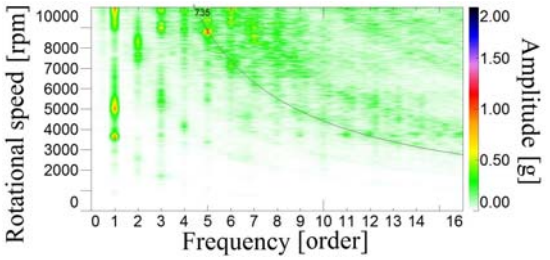

Fig. 17. OSA graph showing vibration acceleration amplitudes measured in the X direction at the second ceramic bearing support

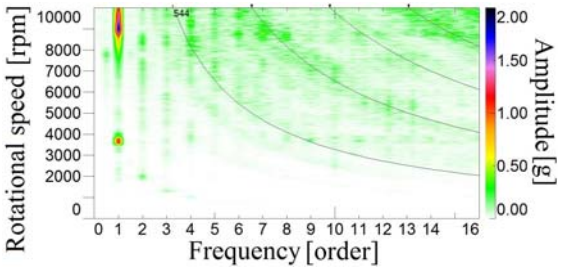

Fig. 18. OSA graph showing vibration acceleration amplitudes measured in the Y direction at the second ceramic bearing support

In the previous cases, looking at the vibrations registered at the second bearing support in the X direction, there were no clear signs that the rotor's operation was no longer stable. The situation is different in the case of all-ceramic bearings (Fig. 17). The first five harmonics could have been observed in this figure. Their maximal acceleration amplitudes are as follows: 1X – 0.72 g and 5X – 0.93 g. The vibrations of the test rig's structure (735 Hz) have had an adverse impact on the operation of the rotor itself. At a synchronous speed with the rotational speed of the rotor, two critical speeds were noticed that were less clearly displayed in previous cases. In the second direction, namely the Y direction, the first harmonic clearly manifested itself (Fig. 18) and the vibrations of the test rig as well (544 Hz). Furthermore, the subharmonic 0.46X made its appearance at the speed of 7,790 rpm, which is a symptom of an unstable operation of hydrodynamic bearings. The unstable operation of the rotor had its effect on the bearings and this might have been possible due to the existing clearance between the bearings' components. The maximal values of the vibration acceleration amplitudes were 0.95 g and 1.41 g at the rotational speeds of 3,730 rpm and 9,050 rpm, respectively.

The graph that is shown in Fig. 19 presents the amplitudes of the rotor's displacements in the X and Y directions. It can be seen that the character of vibrations is very different from that of the other cases. The amplitude values became higher in both directions. It is recalled that, for all-steel and ceramic-steel-hybrid bearings, the amplitudes registered in the X direction were much lower from those registered in the Y direction. This time the highest amplitude was 1.8 mm and it occurred in

the X direction. This amplitude is higher by approximately 327% as compared to all-steel bearings where it had the value of 0.55 mm. In the Y direction, the maximum amplitude has increased by around 185% (from 0.92 mm to 1.71 mm) as compared to the reference value. As was also observed for other bearing types, a stable operation of the system starts from the speed around 2,100 rpm. The large jumps of the values registered in the X direction are observed in Fig. 19, which is also the case for ceramic-steel-hybrid bearings (but not the case for all-steel bearings).

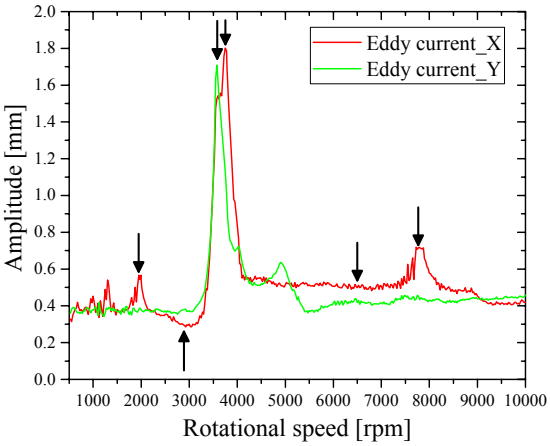

Fig. 19. Amplitude of the rotor's displacement measured at the disk's location (in the X and Y direction) vs. rotational speed

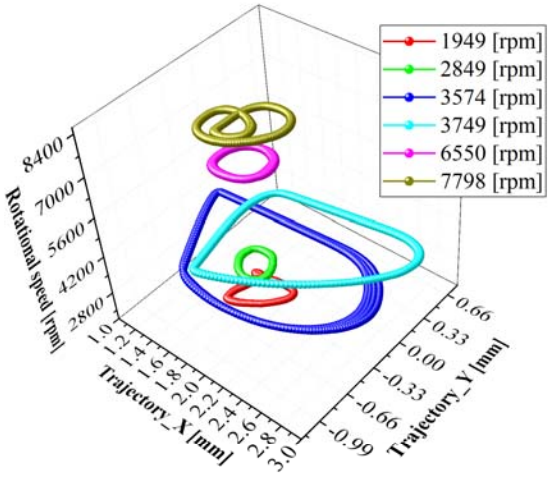

Fig. 20. Trajectories of absolute vibrations at different rotational speeds

On the basis of the results presented in Fig. 8, Fig. 14 and Fig. 20, it can be stated that the vibration trajectories obtained for the rotor supported by all-ceramic bearings are very similar in shape and size (for almost all speeds, not including the resonant speed) to those obtained for other bearing types. At the resonant speed (Fig. 20), the vibration amplitude is visibly higher and, additionally, the vibration trajectory has a very rarely encountered shape—it appears as if the rotor bounced back after striking a hard obstacle. It was probably due to the considerable clearances of the all-ceramic bearings. The rotor (except, of course, for its rotating movement) was free to move within these clearances.

4. CONCLUSIONS

Following the analysis of the information presented above, all three kinds of bearings were compared with each other in terms of their construction. It was established why the symptoms of too high clearance are present on one graph relating to all-ceramic bearings. And the reason for this is the fact that the bearing cage is of the type "TxHB", whereas in other cases it is of the type "J". The use of the flexible rotor and the heavy disk positioned in the middle was a good choice because high vibration amplitudes allowed identifying the characteristics of the bearings but this was also a considerable obstacle to the analysis of the dynamic performance of the rotor. The methods for visualising vibrations shown in this article (OSA graphs and 3D trajectory plots) meet today's standards, and allow for a more detailed insight into the operation of the rotor–bearings system. On the basis of studies carried out, it seems that ceramic-steel-hybrid bearings are a good choice for microturbines. The vibration amplitudes observed for the rotor supported by such bearings are of a similar level to those measured in the case of all-steel bearings. Moreover, the vibration trajectories are of a similar shape for both all-steel and ceramic-steel-hybrid bearings. Therefore, an assumption can be made, with a substantial degree of probability, that if such hybrid bearings were to be applied in a microturbine in which there is a high temperature (approximately 200 °C), vibration amplitudes would have lower values because the bearings' clearances would decrease.

SOURCE OF FUNDING

The research was conducted within the framework of project no. POIG.01.03.01-00-027/08 entitled: "Model agroenergy complexes as an example of distributed cogeneration based on local renewable energy sources".

LITERATURE

1. Zywica G, Kicinski J, Kaczmarczyk TZ, Ihnatowicz E, Turzynski T, Bykuc S. Prototype of the domestic CHP ORC system : construction and experimental research. 3rd Int. Semin. on ORC Power Syst. ASME ORC 2015, Brussels (Belgium), Oct. 12-14, no. 2011, p. Paper ID: 58, Page 1-9, 2015.
2. Kaczmarczyk TZ, Ihnatowicz E, Bykuć S, Żywica G, Kozanecki Z. Experimental investigation of the orc system in a cogenerative domestic power plant with a microturbine and an expansion valve. ASME ORC 2013, 2nd Int. Semin. ORC Power Syst. Oct. 7th – 8th, 2013, Doelen, Rotterdam, Netherlands.

3. Kaczmarczyk TZ, Zywica G, Ihnatowicz E. Experimental investigation of a radial microturbine in organic Rankine cycle system with hfe7100 as working fluid. 3rd International Seminar on ORC Power Systems, ASME ORC 2015, Brussels (Belgium), October 12-14, 2015.
4. Ihnatowicz E, Kaczmarczyk TZ, Żywica G. Vibroacoustic diagnostics of a radial microturbine and a scroll expander operating in the organic Rankine cycle installation. Jve - International Journal of Vibroengineering, 2016; 18(6): 4130–4147.
5. Howard AS. Rotordynamics and Design Methods of an Oil-Free Turbocharger', no. January, 1999.
6. Kiciński J, Zywica G. Steam microturbines in distributed cogeneration. Steam Microturbines in Distributed Cogeneration, 2014: 1–219.
7. Kiciński J. Rotor dynamics. Gdańsk: IMP PAN Publishers, 2006.
8. Beach WP, Dell J. Ceramic Technology Insertion, 1995: 1–12.
9. Adachi K, Kato K, Chen N. Wear map of ceramics. Wear, 1997; 203–204: 291–301.
10. Hsu SM. Shen M. Wear prediction of ceramics. Wear, 2004; 256(9–10): 867–878.
11. Ohta H, Kobayashi K. Vibrations of Hybrid Ceramic Ball Bearings. J. Sound Vib. 1996; 192(2): 481–493.
12. Nosaka M, Oike M, Kikuchi M, Mayumi T. Tribo-Characteristics of Cryogenic Hybrid Ceramic Ball Bearings for Rocket Turbopumps: Self-Lubricating Performance. Tribol. Trans., 1997; 40(1):21–30.
13. Nosaka M, Kikuchi M, Oike M, Kawai N. Tribo-Characteristics of Cryogenic Hybrid Ceramic Ball Bearings for Rocket Turbopumps : Bearing Wear and Transfer Film, 1999; 42(1): 106–115.
14. Tanimoto K, Kajihara K, Yanai K. Hybrid Ceramic Ball Bearings for Turbochargers. SAE International, 2000.
15. Shoda Y, Ijuin S, Aramaki H, Yui H, Toma K. The Performance of a Hybrid Ceramic Ball Bearing Under High Speed Conditions with the Under-Race Lubrication Method. Tribol. Trans., 1997; 40(1): 676–684.
16. Hosang G. Results and design techniques from the application of ceramic ball bearings to the Meradcom 10 kW turbine. 23rd Joint Propulsion Conference, American Institute of Aeronautics and Astronautics, 1987.
17. Bagiński P, Breńkacz Ł. Experimental and simulational modal analysis of the supporting structure of the test rig designed for testing small rotors, which was conducted using electromagnetic vibration exciters. Comparison with the results of the analysis carried out with the use of an impact hammer., Gdańsk, IMP PAN internal report no. 140/2012, 2012. Polish.

Received 2017-01-10
Accepted 2017-02-20
Available online 2017-03-23

Paweł BAGIŃSKI, MSc Eng., works as the assistant at the Institute of Fluid-Flow Machinery in Gdańsk. His main research interests generally include dynamics of rotating machines supported by gas bearings (mainly foil bearings), slide bearings and rolling bearings and diagnostics of structures and machine parts (e.g. modal analysis of the supporting structure of a turbine).

Artur ANDREARCZYK, MSc Eng., works as the assistant at the Institute of Fluid-Flow Machinery in Gdańsk. His main research interests generally include dynamics of rotating machines and using rapid prototyping technology in manufacturing of machine parts.

Grzegorz ŻYWICA, PhD, Eng. Since 2005 has been working at the Institute of Fluid Flow Machinery, Polish Academy of Sciences in Gdańsk. He is the Head of the Department of Turbine Dynamics and Diagnostics. His scientific work focuses on: computational simulation, designing of rotating machinery and bearing systems, rotor dynamics, modal analysis and technical diagnostics.